An Adaptive Eigendeformation-based Reduced-Order Homogenization Model for Composite Materials under Volumetric and Interfacial Damage

Min Lin ∗
University of Wyoming, Laramie, Wyoming, 82071, US

David Brandyberry †
University of Illinois Urbana-Champaign, Champaign, IL, 61801, US

Xiang Zhang ‡
University of Wyoming, Laramie, Wyoming, 82071, US

In this manuscript, we present a multiscale Adaptive Reduced-Order Modeling (AROM) framework to efficiently simulate the response of heterogeneous composite microstructures under interfacial and volumetric damage. This framework builds on the eigendeformation-based reduced-order homogenization model (EHM), which is based on the transformation field analysis (TFA) and operates in the context of computational homogenization with a focus on model order reduction of the microscale problem. EHM pre-computes certain microstructure information by solving a series of linear elastic problems defined over the fully resolved microstructure (i.e., concentration tensors, interaction tensors) and approximates the microscale problem using a much smaller basis spanned over subdomains (also called parts) of the microstructure. Using this reduced basis, and prescribed spatial variation of inelastic response fields over the parts, the microscale problem leads to a set of algebraic equations with part-wise responses as unknowns, instead of node-wise displacements as in finite element analysis. The volumetric and interfacial influence functions are calculated by using the Interface enriched Generalized Finite Element Method (IGFEM) to compute the coefficient tensors, in which the finite element discretization does not need to conform to the material interfaces. AROM takes advantage of pre-computed coefficient tensors associated with the finest ROM and efficiently computes the coefficient tensors of a series of gradually coarsening ROMs. During the multiscale analysis stage, the simulation starts with a coarse ROM which can capture the initial elastic response well. As the loading continues and response in certain parts of the microstructure starts to localize, the analysis adaptively switches to the next level of refined ROM to better capture

∗Graduate student, Department of Mechanical Engineering, email: mlin4@uwyo.edu
†Department of Aerospace Engineering, now System Design Engineer at Lockheed Martin, email: brandyb2@illinois.edu
‡Assistant Professor, Department of Mechanical Engineering, corresponding author email: xiang.zhang@uwyo.edu, member AIAA

those local responses. The performance of AROM is evaluated by comparing the results with regular EHM (no adaptive refinement) and IGFEM under different loading conditions and failure modes for various 2D and 3D microstructures. The proposed AROM provides an efficient way to model history-dependent nonlinear responses for composite materials under localized interface failure and phase damage.

Nomenclature

$\mathbf{y}$	=	Coordinates of the microscale domain
$\bar{\mathbf{u}}, \bar{\boldsymbol{\epsilon}}, \bar{\boldsymbol{\sigma}}$	=	macroscopic displacement, strain, stress
$\tilde{\boldsymbol{\epsilon}}, \tilde{\mathbf{u}}$	=	strain perturbation and displacement perturbation
$\boldsymbol{\epsilon}^{(\alpha)}, \boldsymbol{\mu}^{(\alpha)}, \boldsymbol{\sigma}^{(\alpha)}$	=	strain, inelastic strain and stress of part α
$\breve{\mathbf{H}}, \breve{\mathbf{h}}, \tilde{\mathbf{h}}$	=	elastic, interface and phase influence functions
$\mathbf{L}, \mathbf{E}, \mathbf{P}, \mathbf{Q}, \mathbf{T}, \mathbf{C}, \mathbf{D},$	=	coefficient tensors
$\mathbf{I}$	=	Identity tensor
Superscripts		
α, β	=	part number
Subscripts		
i, j, k, l, m, n	=	index

I. Introduction

Composites are widely used in aerospace engineering under extreme conditions, and there is a significant interest in using computational modeling for predictive evaluation and design of composite structures [1]. Among all the challenges associated with the modeling of composite materials, we are particularly interested in: 1) capturing the highly nonlinear behaviors at the microstructural scale that includes both phase damage and interface debonding and; 2) efficiently upscaling from a material microstructure to a structural component. Efforts have been made to accurately capture complex mechanical behaviors at the microstructural scale, such as using Finite Element Method (FEM), Generalized/Extended Finite Element Method (G/XFEM) [2, 3] and their IGFEM variant [4–7], and Fast Fourier Transform (FFT) based methods [8, 9]. However, challenges still remain for efficient upscaling from the microscale to the macroscale due to the prohibitive computational cost.

Several multiscale strategies have been developed to determine both elastic and inelastic responses of a representative volume element (RVE). Among these multiscale methods, computational homogenization methods [10–12] have been developed to upscale the fully resolved microscale response of an RVE to that of a material point in the struc-

tural scale component. While this method is versatile and flexible to account for different macro/microscale structures and microscale constitutive laws, even with sophisticated solver techniques and the most advanced parallel computing resources [13, 14], the high computational cost still prohibits its broader application for engineering applications.

To alleviate the computational cost of computational homogenization, reduced order modeling (ROM) provides a novel way to balance computational cost and efficiency. Different strategies have been developed to achieve model order reduction at the microscale level. These strategies include but not limited to transformation field analysis [15] and its nonuniform transformation extension [16–18], self-consistent clustering analysis [19, 20], proper orthogonal decomposition [21, 22], the wavelet-reduced-order model [23], and recently data-driven techniques [24, 25]. Alternatively, the eigendeformation-based reduced-order homogenization model (EHM) based on transformation field analysis [26] (TFA), has been proposed to model heterogeneous materials using a hierarchical model-order reduction strategy [27]. EHM has been further extended to model plasticity [28–33], and both continuum and discrete damages [34, 35]. EHM pre-computes certain microstructure information by solving a series of linear elastic problems defined over the fully resolved microstructure (i.e., concentration tensors, interaction tensors) and approximates the microscale problem using a much smaller basis spanned over subdomains (also called parts) of the microstructure. Using this reduced basis, and prescribed spatial variation of inelastic response fields over the parts, the microscale problem leads to a set of algebraic equations with part-wise responses as unknowns, instead of node-wise displacement as in finite element analysis.

Recently, IGFEM has been used to solve the influence functions in EHM, and a penalty method is developed to achieve a single global stiffness matrix for all the elastic, phase inelastic, and interface inelastic influence functions for higher efficiency [36]. In addition, a new interface traction formation is proposed, and the response-based partitioning scheme is adopted [19] and extended for interface partitioning. They also systematically studied the response of various composite microstructures, and further demonstrated the potential of using EHM for nonlinear microstructure design [37]. Fig. 1 shows the efficiency and accuracy of EHM compared to the reference IGEFM simulation for a simple particulate composite microstructure under different loading conditions and failure modes. Overall, EHM can capture the stress-strain response reasonably well, with 2-5 orders of magnitude of higher efficiency than IGFEM.

It can also be seen from Fig. 1 that even for ROM with a very small number of parts (e.g., one part for the inclusion, phase or interface), it generally captures the initial response well and a finer ROM is needed at later loading stage. This is expected as ROM assumes a uniform response in each of the parts, and a finer ROM is needed when localized responses emerge in some of the parts. We, therefore, develop an AROM based on EHM for efficient multiscale analysis. During the multiscale analysis stage of AROM, the simulation starts with a coarse ROM which can capture the initial elastic response well. As the loading continues and response in certain parts of the microstructure starts to localize, the analysis adaptively switches to the next level of refined ROM to better capture those local responses. The performance of AROM is evaluated by comparing the results with regular EHM (no adaptive refinement) and IGFEM under different loading conditions and failure modes for various 2D and 3D microstructures.

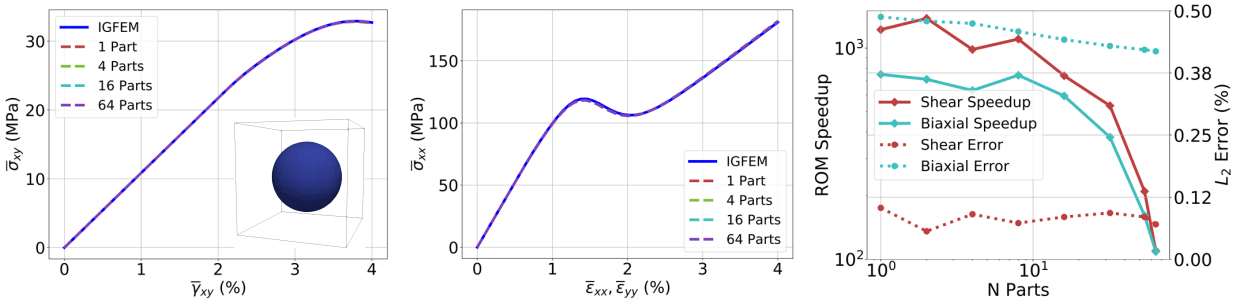

(a) Inclusion Continuum Damage

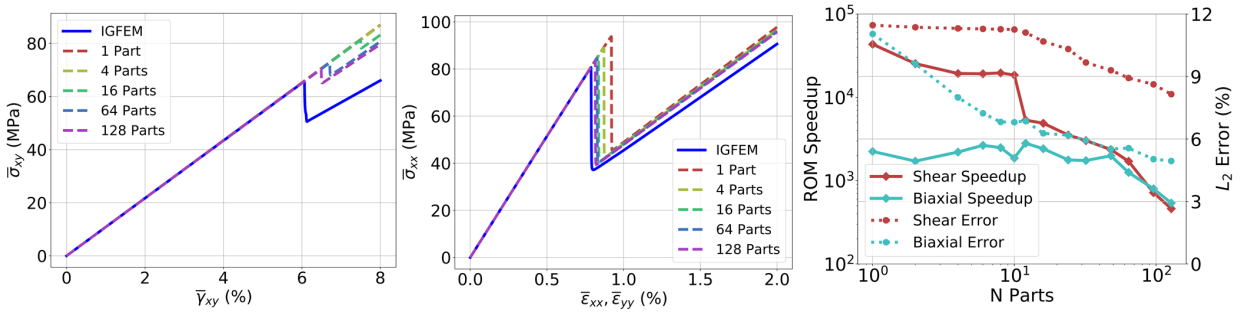

(b) Interface Debonding

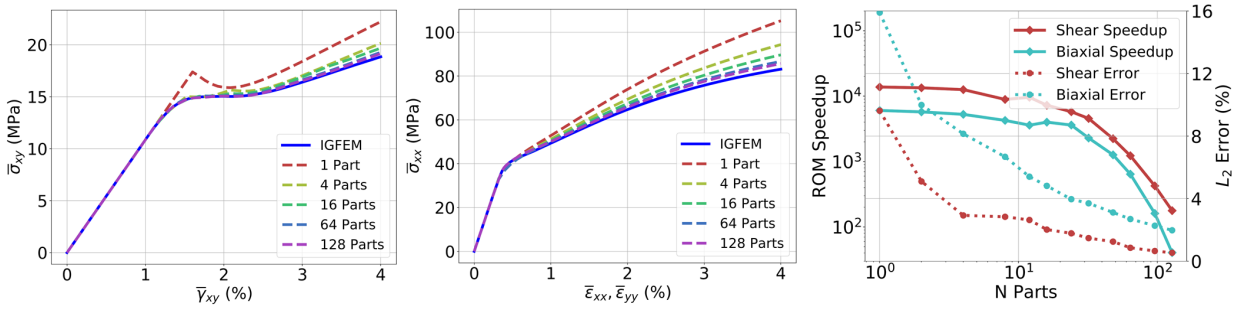

(c) Matrix Continuum Damage

Fig. 1 Accuracy and speedup of EHM with different number parts for a single-inclusion particulate composite microstructure under different loading conditions and failure modes [36]: (a) Inclusion damage; (b) Interface cohesive debonding of particles from the matrix; (c) Matrix damage.

The remainder of the manuscript is organized as follows: Section II overviews the EHM model, and details the AROM refining scheme as well as the calculation of coefficient tensors for coarser ROMs from the finest ROM. Model verification is then conducted in Section III, together with the case study of various 2D and 3D composite microstructures. Section IV summarizes the manuscript.

II. Theory

In this section, an overview of the existing EHM method that considers damage in the matrix, reinforcement, and interface of composite materials is first provided. we then discuss in detail how to construct a series of gradually refining ROMs for use during the multiscale simulation.

A. Overview of EHM

EHM is based on TFA and works in a two-scale computational homogenization setting. EHM reduces the computational cost by: 1) Partition matrix, phase, and interface of the model into a smaller number of subdomains known as parts; 2) A set of coefficient tensors associated with the microstructure partitioning are computed in the pre-processing stage by solving the influence function problems defined over the linear elastic microstructures, which reflect the interactions between the microstructure and parts; 3) Inelastic fields are assumed uniform within each part. With the above treatment and simplifications, the microscale problem leads to a set of algebraic equations with part-wise responses as unknowns. EHM can be used as a constitutive law in a multiscale analysis of an arbitrary macrostructure, or it can be used to investigate the response of a microstructure under a prescribed macroscale loading history. We focus on the latter, where the governing equations in the response of the microscale domain are defined as:

$$
\begin{aligned}
&\sigma_{ij,j}(\boldsymbol{y}) = 0, \quad \boldsymbol{y} \in \Theta \\
&\epsilon_{ij}(\boldsymbol{y}) = \bar{\epsilon}_{ij} + \tilde{\epsilon}_{ij}(\boldsymbol{y}), \\
&\tilde{\epsilon}_{ij}(\boldsymbol{y}) = \frac{1}{2}\left(\tilde{u}_{i,j} + \tilde{u}_{j,i}\right), \\
&\sigma_{ij}(\boldsymbol{y}) n_j(\boldsymbol{y}) = t_i(\llbracket \tilde{\boldsymbol{u}}(\boldsymbol{y}) \rrbracket), \quad \boldsymbol{y} \in \Gamma \\
&\bar{\sigma}_{ij} = \frac{1}{|\Theta|}\int_{\Theta} \sigma_{ij}(\boldsymbol{y}) d\Theta
\end{aligned}
\tag{1}
$$

where the macroscopic stress $\bar{\sigma}_{ij}$ is the numerical average of microscopic stress over the microscale RVE domain Θ. The strain tensor ϵ_{ij} consists of macroscale component $\bar{\epsilon}_{ij}$ and perturbation component $\tilde{\epsilon}_{ij}$. $\tilde{u}_i$ is defined as perturbation displacement, which is periodic in RVE. $\mathbf{y}$ is the microstructural coordinates, and the $|\cdot|$ operator indicates the area (2D) or volume (3D) of the microstructure domain Θ. The last equation in 1 relates the cohesive tractions t_i, caused by displacement jumps along material interfaces, Γ.

The volumetric domain that is damageable can be partitioned into $\tilde{N}$ volumetric parts, represented by $\Theta^{[\alpha]}$ ($\alpha = 1, 2, , \tilde{N}$), and the imperfect material interfaces can be partitioned into $\check{N}$ parts, denoted by $\Gamma^{[\xi]}$ ($\xi = 1, 2, \check{N}$). EHM relates the perturbation displacement field by so-called elastic ($\mathbf{H}$), phase inelastic ($\check{\mathbf{h}}$), and interface inelastic ($\tilde{\mathbf{h}}$) influence functions, which are computed by solving a series of linear elastic problems over the microscale domain using IGFEM [36]. The perturbation field can be defined as:

$$
\tilde{u}_i(\boldsymbol{y}) = H_i^{kl}(\boldsymbol{y})\bar{\epsilon}_{kl} + \sum_{\xi=1}^{N} \check{h}_i^{n[\xi]}(\boldsymbol{y})\delta_n^{[\xi]} + \sum_{\xi=1}^{\tilde{N}} \tilde{h}_i^{kl[\alpha]}(\boldsymbol{y})\mu_{kl}^{[\alpha]} \tag{2}
$$

where $\mu_{kl}^{[\alpha]}$ is the inelastic in the phase part α and $\delta_n^{[\xi]}$ is the displacement jump in the interface part ξ. The EHM system for composite materials is summarized in Box 1 and details are in Ref. [36]. For the constitutive equations for the nonlinear phase parts and traction-separation laws for the interface parts, while depending on user specification,

we adopt the exponential cohesive-zone model (CZM) of Ortiz and Pandolfi [38], and the isotropic continuum damage model presented by Simo and Ju [39].

- Residual of balancing strain in a phase part:

$$R_1^{(\beta)} = E_{ij}^{kl[\beta]}\bar{\epsilon}_{kl} + \sum_{\alpha=1}^{\tilde{M}} P_{ij}^{kl[\beta\alpha]}\mu_{kl}^{[\alpha]} + \sum_{\xi=1}^{\check{M}} O_{ij}^{m[\beta\xi]}\delta_m^{[\xi]} - \epsilon_{ij}^{[\beta]} = 0, \forall\beta \in [1, \tilde{N}]$$

- Residual of balancing tractions in an interface part:

$$R_2^{(\eta)} = t_n^{[n]} - \sum_{\alpha=1}^{\tilde{M}} C_n^{kl[\eta\alpha]}\mu_{kl}^{[\alpha]} - \sum_{\xi=1}^{\check{M}} D_n^{m[\eta\xi]}\delta_m^{[\xi]} - T_n^{kl[\eta]}\bar{\epsilon}_{kl} = 0, \forall\eta \in [1, \check{N}]$$

- Coefficient tensors:

$$E_{ij}^{kl[\beta]} = I_{ijkl} + \frac{1}{|\Theta^{[\beta]}|}\int_{\Theta^{[\beta]}} H_{(i,y_j)}^{kl}(\boldsymbol{y})d\Theta$$

$$P_{ij}^{kl[\beta\alpha]} = \frac{1}{|\Theta^{[\beta]}|}\int_{\Theta^{[\beta]}} \tilde{h}_{(i,y_j)}^{kl[\alpha]}(\boldsymbol{y})d\Theta$$

$$O_{ij}^{m[\beta\xi]} = \frac{1}{|\Theta^{[\beta]}|}\int_{\Theta^{[\beta]}} \check{h}_{(i,y_j)}^{m[\xi]}(\boldsymbol{y})d\Theta$$

$$T_n^{kl[\eta]} = \frac{1}{|\Gamma^{[\eta]}|}\int_{\Gamma^{[\eta]}} Q_{ni}(\boldsymbol{y})L_{ijpq}(\boldsymbol{y})\left[H_{(p,y_q)}^{kl}(\boldsymbol{y}) + I_{pqkl}(\boldsymbol{y})\right]\bar{n}_j(\boldsymbol{y})d\Gamma$$

$$C_n^{kl[\eta\alpha]} = \frac{1}{|\Gamma^{[\eta]}|}\int_{\Gamma^{[\eta]}} Q_{ni}(\boldsymbol{y})L_{ijpq}(\boldsymbol{y})\left[\tilde{h}_{(p,y_q)}^{kl[\boldsymbol{y})}(\boldsymbol{y}) - I_{pqkl}^{[\alpha]}(\boldsymbol{y})\right]\bar{n}_j(\boldsymbol{y})d\Gamma$$

$$D_n^{m[\eta\xi]} = \frac{1}{|\Gamma^{[\eta]}|}\int_{\Gamma^{[\eta]}} Q_{ni}(\boldsymbol{y})L_{ijpq}(\boldsymbol{y})\check{h}_{(p,y_q)}^{m[\xi]}(\boldsymbol{y})\bar{n}_j(\boldsymbol{y})d\Gamma$$

Box 1 Summary of the reduced order microscale problem.

B. ROM Partitioning

ROM are approximations of high-fidelity simulations. One of the key characteristics of this approach is that it provides a hierarchical sequence of ROMs ranging from low fidelity - high efficiency to high fidelity - low efficiency models, by increasing the number of parts, such that computational performance characteristics of the ROMs can be directly controlled. The idea of static and dynamic partitioning was conceptually discussed [27]. Static partitioning refers to the parts being pre-defined and fixed, and the same ROM is used throughout the multiscale analysis. Dynamic partitioning, on the other hand, computes and stores element-wise influence functions and allows the computation of coefficient tensors for arbitrary partitioning on the fly (see coefficient tensors in Box 1) and can switch to a new ROM during the multiscale analysis. The majority of ROMs are based on static partitioning, where one needs to split the damageable phase regions and imperfect interfaces into a desired number of parts, and select their geometries.

When the ROM order (i.e., number of parts) is fixed, it is desirable to achieve the lowest error using optimal partitioning of the microstructure. Geometry- and response-based partitioning of the microstructure are the most frequently used partitioning strategies, which either uses the distinct geometry features (e.g., inclusions and matrix in composites and grains in metals [28, 40–42]) of the microstructure to construct a part, or group regions of similar response when

subjecting the microstructure to a given loading into a part [19, 43]. Optimization can also be used to determine the optimal partitioning of the microstructure [44, 45]. Brandyberry et al. [36] adopted the response-based k-means clustering of phase parts [19], and extended it to interface partitioning. This partitioning scheme creates parts not necessarily geometrically connected and is very flexible to use (i.e., only need to specify the number of parts), and this scheme will be adopted in the current study. Details about these damage models are summarized in Ref. [36].

Inspired by mesh adaptivity in FEA [46, 47], and the observation from Fig. 1 that a coarse ROM is sufficient to capture initial response while a finer ROM is desired when localized response emerges, we aim to develop an AROM based on EHM. Fan et al. [48] developed an adaptive two-scale nonlinear homogenization method, where computational homogenization and a single ROM are used at different locations of the macrostructure. Recently, Ferreira et al. Ferreira et al. [49] proposed an Adaptive Self-Consistent Clustering Analysis (ASCA) method to predict the plasticity and fracture behaviors of particle-matrix composites, which demonstrates that this strategy can improve the accuracy while remaining low computation cost. But this study does not consider interface damage and adopted a relatively simple failure criterion for the phases.

C. AROM based on EHM with volumetric and interfacial damage

Our proposed AROM is based on EHM and considers both volumetric and interfacial damages. While one could take the dynamic partitioning concept, and only refine selected parts as needed, we limit our consideration in the current work to an adaptive refinement scheme that every coarse part will be refined to the user-specified level. Coarser ROM parts are based on the grouping of the finest ROM parts through k-means clustering. In the pre-processing stage, we first compute the coefficient tensors of the finest ROM and store the k-means partitioning information of coarser ROMs. Based on that, the coefficient tensors of the coarser ROMs can be computed on the fly during the simulation process. When the multiscale simulation starts, the coarsest ROM will be used which is expected to capture the initial elastic response accurately. As the load continues, deformation and damage in certain parts start to accumulate, and the simulation switches to the next level of refined ROM based on a refining threshold and state initialization rule.

Figure 2 schematically illustrates the construction of a series of gradually refining ROMs using an idealized two-phase microstructure. Each color indicates a different material phase, while the black grid lines indicate part boundary and white grids represent element edges. The user specifies the part numbers of a series of adaptively refining ROMs to be used in the simulation for all phases (e.g., the adaptive part number list is (2,4,...,16) for two phases in Fig. 2). We then first calculate the coefficient tensors of the finest ROM (Fig. 2d) during the pre-processing. In the multiscale simulation, we start with the 2-part coarsest ROM (one-part-per-phase, Fig. 2b), and the coefficient tensors of this ROM can be computed from the finest ROM using k-means clustering [19, 36] of the localization tensors (i.e., $\mathbf{E}^{[\beta]}$ in Box 1) based on the finest 16-part ROM. The next level of coarse ROM (4-part) (Fig. 2c) can be computed in the same way. This coarsening scheme will ensure that each parent part will be split into the desired number of children parts during

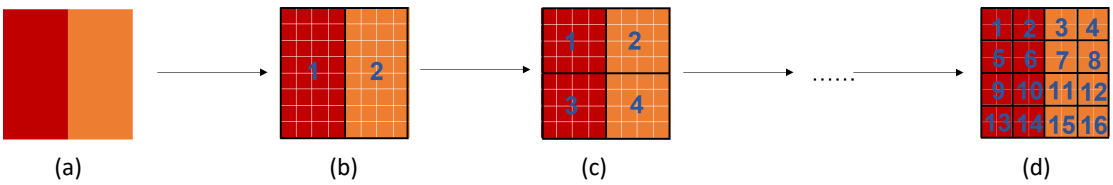

Fig. 2 Schematic illustration of AROM refinement of (a) a two-phase microstructure, which starts with (b) 2-part, then to (c) 4-part, and finally to (d) 16-part ROM. Black lines show part boundaries while white lines indicate element edges.

the refining, and the children parts' deformation state can be straightforwardly initialized using their parent state. The interface partitioning/refinement takes a similar approach as the phases.

The calculations of coefficient tensors of a large number of ROMs could be computationally expensive, and we leverage the spitting of a parent part into children parts for fast calculation of coefficient tensors of the coarser ROMs using those of the finest ROM as illustrated in Box. 2. While more sophisticated refining criteria could be developed, we consider refinement when the load reaches user-specified values in the current study.

- Coefficient tensors related to only phase parts::

$$P^{(\beta\alpha)} = \frac{1}{\sum_{k=1}^{N_\beta} \left|\Theta^{(\beta_k)}\right|} \sum_{k=1}^{N_\beta} \sum_{i=1}^{N_\alpha} \left|\Theta^{(\beta_k)}\right| P^{(\beta_k \alpha_i)}$$

$$E_{ij}^{kl(\beta)} = \frac{1}{\sum_{r=1}^{N_\beta} \left|\Theta^{(\beta_r)}\right|} \sum_{r=1}^{N_\beta} \left|\Theta^{(\beta_r)}\right| E_{ij}^{kl(\beta_r)}$$

$$A_{ijkl}^{(\alpha)} = \sum_{s=1}^{N_\alpha} A_{ijkl}^{(\alpha_s)}$$

- Coefficient tensors related to only interface parts:

$$D_n^{m(\eta\xi)} = \frac{1}{\sum_{s=1}^{N_\eta} \left|\Gamma^{(\eta_s)}\right|} \sum_{s=1}^{N_\eta} \left|\Gamma^{(\eta_s)}\right| \sum_{r=1}^{N_\xi} D_n^{m(\eta_s \xi_r)}$$

$$T_n^{kl(\xi)} = \frac{1}{\sum_{r=1}^{N_\xi} \left|\Gamma^{(\xi_r)}\right|} \sum_{r=1}^{N_\xi} \left|\Gamma^{(\xi_i)}\right| T_n^{kl(\xi_r)}$$

$$\bar{B}_{ijn}^{(\xi)} = \sum_{r=1}^{N_\xi} \bar{B}_{ijn}^{(\xi_r)}$$

- Coefficient tensors related to both interface and phase parts:

$$C_n^{kl[\eta\alpha]} = \frac{1}{\sum_{s=1}^{N_\eta} \left|\Gamma^{(\eta_s)}\right|} \sum_{s=1}^{N_\eta} \left|\Gamma^{(\eta_s)}\right| \sum_{r=1}^{N_\alpha} C_n^{kl(\eta_s \alpha_r)}$$

$$O_{ij}^{m(\beta\xi)} = \frac{1}{\sum_{s=1}^{N_\eta} \left|\Theta^{(\beta_s)}\right|} \sum_{s=1}^{N_\beta} \sum_{r=1}^{N_\xi} \left|\Theta^{(\beta_s)}\right| O_{ij}^{m(\beta_s \xi_r)}$$

Box 2 Computing coefficient tensors of coarse ROM from the finest ROM.

III. Numerical Verification

In this section, we investigate a series of examples to probe the efficiency and accuracy of AROM. The first two examples are based on a 3D composite model, a sphere reinforcement inclusion of radius 35 μm inside a cubic representative volume element (RVE) with a side length of 100 μm. These two examples are under biaxial loading conditions but with different failure modes. We consider continuum damage in the matrix and cohesive damage in the particle interface. The third example is a particulate composite RVE that contains ten randomly distributed spherical particles. Each particle is with a radius of 3.5 μm. This model is under a tri-axial macroscopic loading. The last example is a 90^o unidirectional composite ply with complex geometries. In this model, a composite laminate that contains 575 circular fibers is under a pure shear loading, and the interface failure is considered.

A. A particulate composite microstructure with a single spherical inclusion with matrix damage

We consider a particulate composite microstructure with a single spherical inclusion inside the epoxy matrix as shown in the insert of Fig. 3b. For the spherical inclusion, it is an isotropic material with Young's modulus of 12 GPa and Poisson's ratio of 0.4. The matrix is an isotropic epoxy matrix with Young's modulus of 2.4 GPa and Poisson's ratio of 0.4. The matrix damage parameters for the continuum damage are $Y_{in} = 0.15$ MPa, $\mu = 20\ s^{-1}$, $P_1 = 15$, and $P_2 = 0.4$. The 3D RVE is subjected to biaxial tension loads where $\bar{\epsilon} = \{0.04, 0.04, 0, 0, 0, 0\}$.

Results of AROM, ROM, and reference IGFEM simulation are compared in Fig. 3b. In adaptive ROM (AROM), it begins with 2 matrix phase parts, switches to 4 parts at simulation time step $t = 0.5$, and continues refinement to 16 parts at $t = 0.7$. The three matrix phase partitionings for AROM are shown in Fig. 3a. The corresponding stress-strain curves of AROM, ROM, and IGFEM are shown in Fig. 3b. As seen from 3b, in the first switch point of AROM where the macroscopic strain amplitude is near 0.013, the AROM model is refined into 4 parts. We can see there is a clear stress drop in the first switch point. We also can find a similar drop at the second switch point where strain amplitude is around 0.025. After the second switch point, AROM finally converges to the results of ROM with 16 matrix parts. When compared with IGFEM results, the accuracy of AROM is comparable to 16-part ROM. AROM achieves better accuracy than 2-part ROM and 4-part ROM. The computation time of AROM to solve the residual problems defined in Box 1 is about 0.19 CPU seconds while that of 16-part ROM is about 0.36 CPU seconds, which indicates AROM is nearly 2 times faster than 16-part ROM for this simple RVE.

B. A particulate composite microstructure containing a single spherical inclusion with interface damage

The second example has the same model geometry, elastic material properties, and loading condition as in the last section. But here only the interface damage is considered, and the damage parameters for Ortiz-Pandolfi Cohesive Zone Model are $\sigma_c = 100$ MPa and $\delta_c = 20\ nm$.

AROM begins with a coarse ROM with 2 interface parts, then 4 interface parts, and finally the finest ROM with

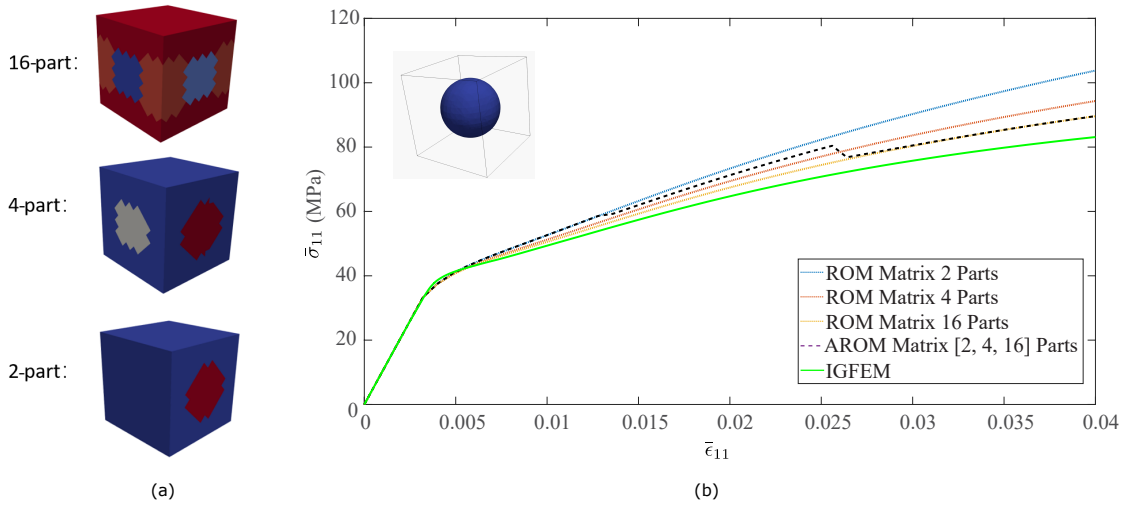

Fig. 3 (a) Phase partitioning using 2 parts, 4 parts, and 16 parts in AROM under biaxial loading condition; (b) Stress-strain curves of IGFEM, AROM (from 2 to 16 phase parts) and ROM (2, 4, and 16 phase parts).

16 interface parts. The interface partition history for AROM is shown in Fig. 4a. We use the same refinement switch points at timestep t = 0.5 and 0.7 as in the previous example. In the switch points, the interface parts are refined from 2 interface parts to 4 parts, and 4 parts to 16 parts, respectively. The stress-strain curves of AROM, ROM, and IGFEM in the 11 direction are shown in Fig. 4b, and the zoomed version of the rectangular black box in Fig. 4b is shown in Fig. 4c. From Fig. 4c, AROM demonstrates similar drops in the switch points as in the previous matrix damage case. AROM converges to the 16-part ROM results. The computation time of AROM to solve the residual problems is about 0.07 s while that of 16-part ROM is about 0.11 s. AROM achieves a 1.5x speedup compared with ROM with 16 interface parts.

C. 3D particulate composites containing ten spherical inclusions

ROM can be used to compute models with complicated geometries. The example presented here is a 3D particulate composite that is composed of ten randomly distributed spherical inclusions. It considers all three types of damages: matrix, inclusion, and interface damages under tri-axial loads. The macroscopic strain load is $\bar{\epsilon}$ = {0.04,-0.02,-0.02,0,0,0}. In this example, the matrix continuum damage parameters are Y_{in} = 0.15 MPa, μ = 20 s^{-1}, P_1 = 10, and P_2 = 0.2, and the inclusion damage parameters are Y_{in} = 0.15 MPa, μ = 20 s^{-1}, P_1 = 5, and P_2 = 0.5. The cohesive damage parameters are σ_c = 100 MPa and δ_c = 20 nm.

Adaptive strategy is applied for both phase parts (matrix and inclusion) and interface parts (particle interface). The adaptive part lists for matrix, inclusion and interface are [5,10,15], [6,12,24], and [7,14,28], respectively. ROM is with 15 matrix parts, 24 inclusion parts, and 28 interface parts. The refinement switch points of AROM are the same as in previous examples, t = 0.5 and 0.7. AROM starts with 5 matrix parts, 6 inclusion parts, and 7 interface parts. The stress-strain curves of AROM and ROM are shown in Fig. 5a. At the first switch point, AROM overestimates the

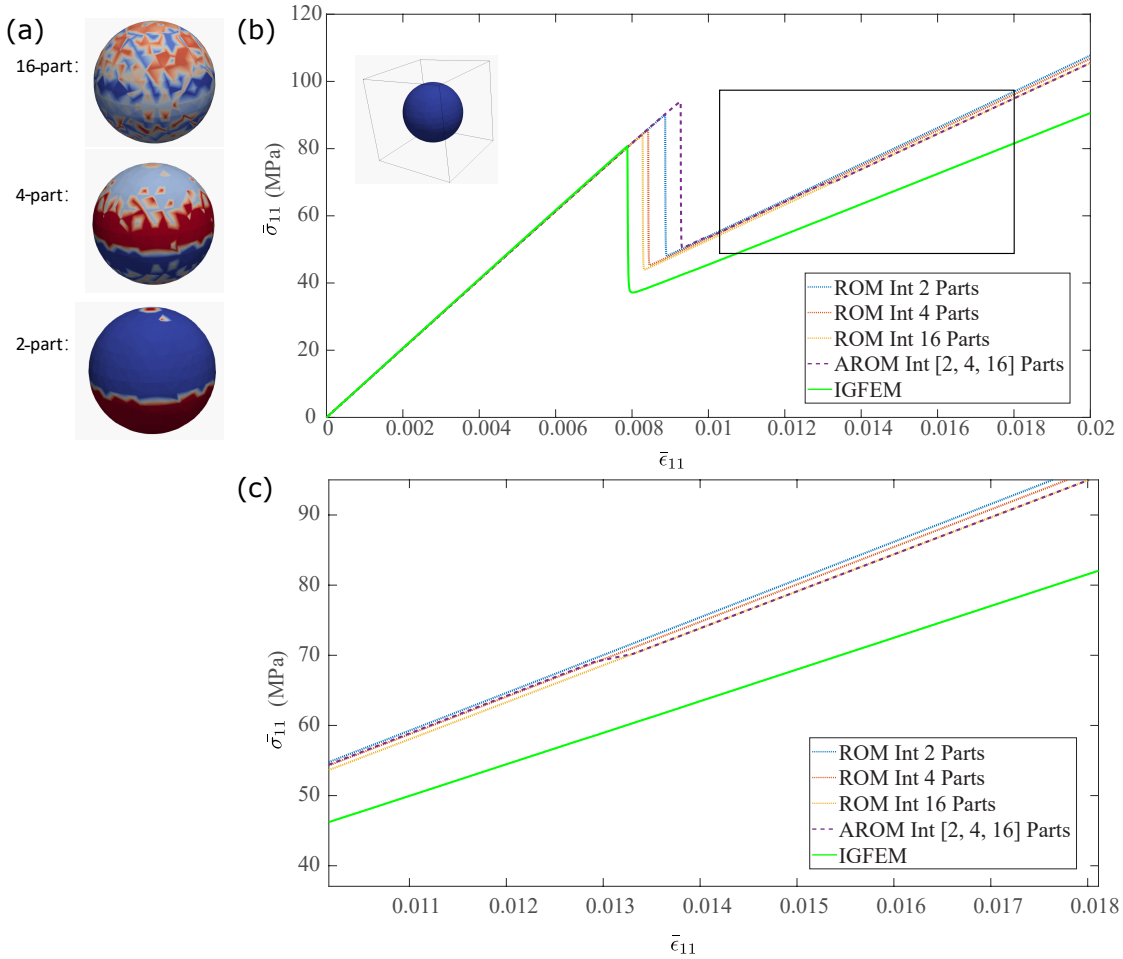

Fig. 4 **(a) Particle interface partitioning i2 parts, 4 parts, and 16 parts in AROM under biaxial loading condition; (b) Stress-strain curves of IGFEM, AROM (from 2 to 4 to 16 interface parts) and ROM (2, 4, and 16 interface parts); (c) Zoomed stress-train curves of the black rectangle area in (b).**

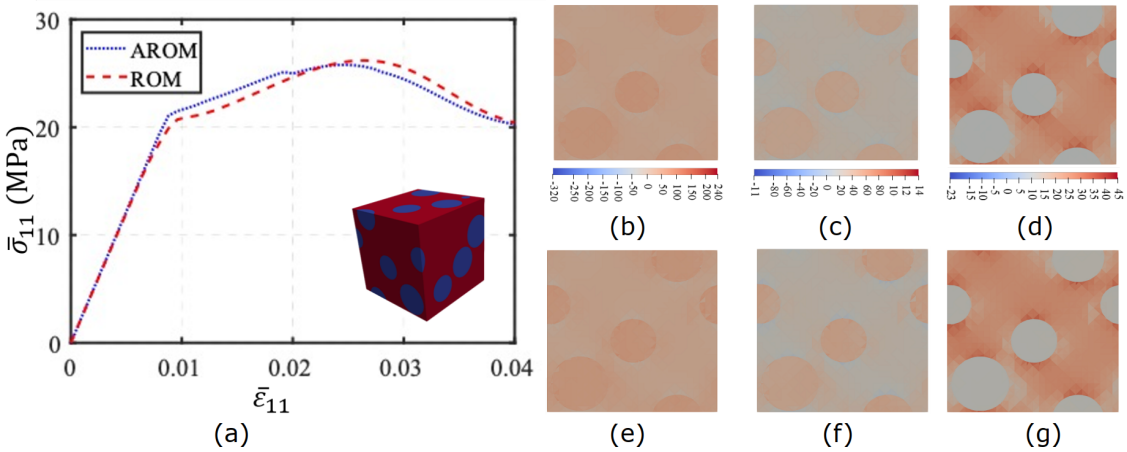

Fig. 5 (a) Stress-strain curves of AROM and ROM considering matrix, damage and interface damage of the particulate microstructure in the insert under tri-axial loading. AROM begins with 5 matrix, 6 inclusion, and 7 interface parts (abbreviated as [5, 6, 7]), then to [10, 12, 14] and finally to [15, 24, 28], while ROM use a constant partition of [15, 24, 28]. Stress contours of AROM before each refining and at the end of the simulation (i.e., t=0.5, 0.7, and 1 s) in (b)-(d), and corresponding ROM results in (e)-(g).

stress response by less than 5% when compared with ROM. And at the second switch point, AROM underestimates the response by about 3%. But the finest AROM finally converges to the ROM results. The stress contours of AROM are illustrated in Fig. 5b-d and that of ROM is illustrated in Fig. 5e-g. It can be seen from Fig. 5b and e, in the first switch point, the overall stress response of AROM is slightly higher than ROM, which conforms to the observation in stress-strain curves. The localized response of the final stress contour at $t = 1.0$ of AROM shown in Fig. 5d demonstrates remarkable agreement with that of ROM shown in Fig. 5g.

D. A composite ply with interface damage

In this subsection, we investigate a model with more complicated geometries. A unidirectional composite ply including 575 circular fibers is shown in Fig. 6a. The cohesive damage model is applied to the fiber interfaces, and the domain is subjected to a pure shear loading with an amplitude of 0.03.

The adaptive interface part list is [4,16,64], and ROM is with 64 interface parts. Fig. 6a demonstrates the $\bar{\sigma}_{12}$ - $\bar{\gamma}_{12}$ curves of AROM and ROM. The localized shear stress distributions in AROM and 64-part ROM are compared in Fig. 6c and d, which shows similar shear stress distributions. And the spatial variations of shear stress along the horizontal red dot lines in Fig. 6c and d are plotted in Fig. 6b. AROM obtains the same local response as ROM.

IV. Summary

We develop an AROM framework to further accelerate EHM for the modeling of composite materials under volumetric and interfacial damage. The user specifies and constructs a series of gradually refining ROMs during the pre-processing stage. During the multiscale analysis, the simulation starts with a coarse ROM that can efficiently and accurately capture the initial response, and switches to a refined ROM when localized response starts to accumulate

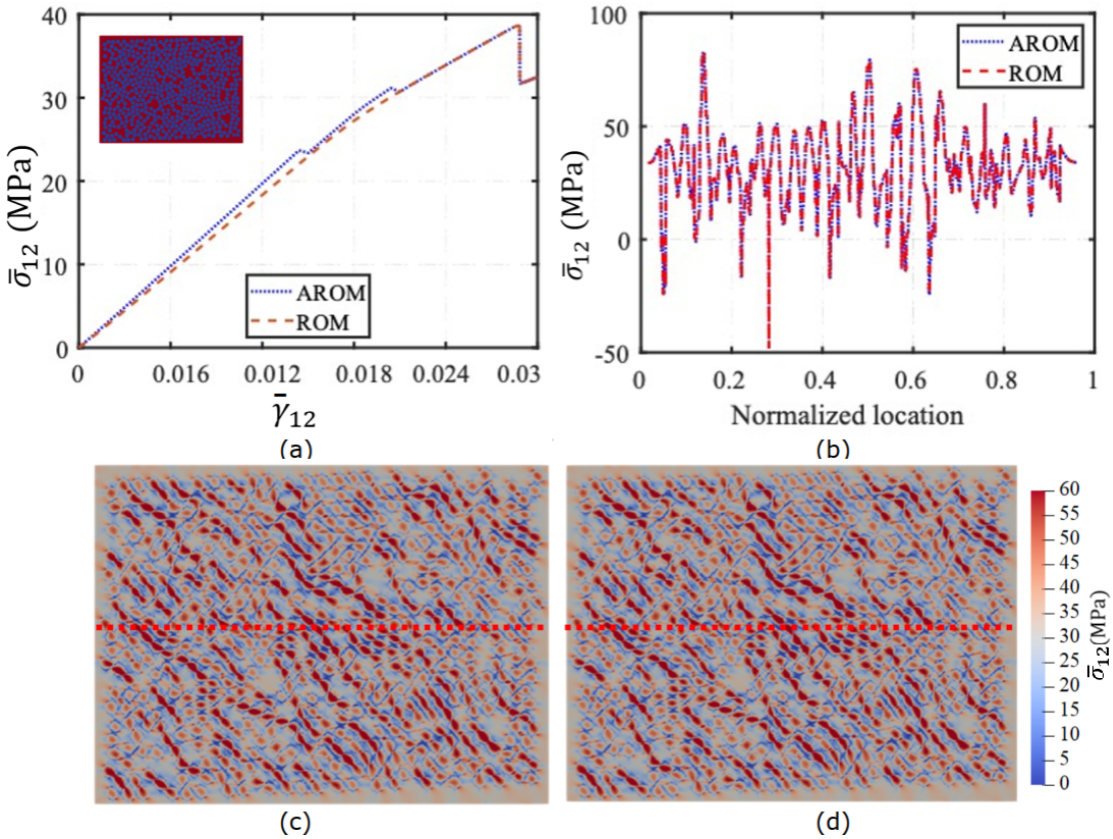

Fig. 6 **(a) Stress-strain curves of AROM and ROM of a 90^o unidirectional composite ply in the insert with interface damage under shear loading. AROM begins with 4 interface parts, then to 16 and finally 64 interface parts. ROM is with 64 interface parts; Shear stress contour of AROM in (c) and ROM in (d), and their spatial distribution along the center line marked in (c) and (d) are compared in (b).**

in some of the ROM parts. A series of numerical examples on different 2D and 3D composite microstructures are analyzed and demonstrate the computational accuracy and efficiency of AROM compared with non-refining ROM and reference IGFEM simulation. Future work focuses on developing non-uniform refinement and more sophisticated refining criteria.

Funding Sources

The authors gratefully acknowledge the research funding from the NSF CMMI Mechanics of Materials and Structures Program (Grant No. 2114822). The authors would also like to thank the computing resources and support from the Advanced Research Computing Center (ARCC) at the University of Wyoming.

References

[1] Lubin, G., *Handbook of Composites*, Springer Science & Business Media, 2013.

[2] Moës, N., Dolbow, J., and Belytschko, T., "A finite element method for crack growth without remeshing," *Int. J. Numer. Methods Eng.*, Vol. 46, No. 1, 1999, pp. 131–150. https://doi.org/10.1002/(SICI)1097-0207(19990910)46:1<131::AID-NME726>3.0.CO;2-J.

[3] Duarte, C. A., Hamzeh, O. N., Liszka, T. J., and Tworzydlo, W. W., "A generalized finite element method for the simulation of three-dimensional dynamic crack propagation," *Comput. Methods Appl. Mech. Eng.*, Vol. 190, No. 15, 2001, pp. 2227–2262. https://doi.org/10.1016/S0045-7825(00)00233-4.

[4] Soghrati, S., and Geubelle, P. H., "A 3D interface-enriched generalized finite element method for weakly discontinuous problems with complex internal geometries," *Comput. Methods Appl. Mech. Eng.*, Vol. 217-220, 2012, pp. 46–57. https://doi.org/10.1016/j.cma.2011.12.010.

[5] Aragon, A. M., and Simone, A., "The Discontinuity-Enriched Finite Element Method," *Int. J. Numer. Methods Eng.*, Vol. 112, 2017, pp. 1589–1613. https://doi.org/10.1002/nme.5570.

[6] Zhang, X., Brandyberry, D. R., and Geubelle, P. H., "IGFEM-based shape sensitivity analysis of the transverse failure of a composite laminate," *Comput. Mech.*, Vol. 64, No. 5, 2019, pp. 1455–1472. https://doi.org/10.1007/s00466-019-01726-y.

[7] Zacek, S., Brandyberry, D., Klepacki, A., Montgomery, C., Shakiba, M., Rossol, M., Najafi, A., Zhang, X., Sottos, N., Geubelle, P., Przybyla, C., and Jefferson, G., *Transverse Failure of Unidirectional Composites: Sensitivity to Interfacial Properties*, Springer International Publishing, Cham, 2020, p. 329–347. https://doi.org/10.1007/978-3-030-40562-5_12.

[8] Moulinec, H., and Suquet, P., "A Fast Numerical Method for Computing the Linear and Nonlinear Mechanical Properties of Composites," *Comptes Rendus de l'Académie des sciences. Série II. Mécanique, physique, chimie, astronomie*, 1994.

[9] Sharma, L., Peerlings, R. H. J., Shanthraj, P., Roters, F., and Geers, M. G. D., "An FFT-based spectral solver for interface decohesion modelling using a gradient damage approach," *Comput. Mech.*, Vol. 65, No. 4, 2020, pp. 925–939. https://doi.org/10.1007/s00466-019-01801-4.

[10] Babuška, I., "HOMOGENIZATION AND ITS APPLICATION. MATHEMATICAL AND COMPUTATIONAL PROBLEMS," *Numerical Solution of Partial Differential Equations–III*, edited by B. Hubbard, Academic Press, 1976, pp. 89–116. https://doi.org/10.1016/B978-0-12-358503-5.50009-9.

[11] Bensoussan, A., Lions, J.-L., and Papanicolaou, G., *Asymptotic Analysis for Periodic Structures*, American Mathematical Soc., 2011.

[12] Miehe, C., Schröder, J., and Schotte, J., "Computational homogenization analysis in finite plasticity Simulation of texture development in polycrystalline materials," *Comput. Methods Appl. Mech. Eng.*, Vol. 171, 1999.

[13] Mosby, M., and Matouš, K., "Computational homogenization at extreme scales," *Extreme Mech. Lett.*, Vol. 6, 2016, pp. 68–74. https://doi.org/10.1016/j.eml.2015.12.009.

[14] Rahul, and De, S., "Analysis of the Jacobian-free multiscale method (JFMM)," *Comput. Mech.*, Vol. 56, No. 5, 2015, pp. 769–783. https://doi.org/10.1007/s00466-015-1200-z.

[15] Dvorak, G. J., "Transformation Field Analysis of Inelastic Composite Materials," *Proceedings: Mathematical and Physical Sciences*, Vol. 437, No. 1900, 1992, pp. 311–327.

[16] Michel, J. C., and Suquet, P., "Nonuniform transformation field analysis," *Int. J. Solids Struct.*, Vol. 40, No. 25, 2003, pp. 6937–6955. https://doi.org/10.1016/S0020-7683(03)00346-9.

[17] Fritzen, F., and Leuschner, M., "Nonlinear reduced order homogenization of materials including cohesive interfaces," *Comput. Mech.*, Vol. 56, No. 1, 2015, pp. 131–151. https://doi.org/10.1007/s00466-015-1163-0.

[18] Leuschner, M., and Fritzen, F., "Reduced order homogenization for viscoplastic composite materials including dissipative imperfect interfaces," *Mech. Mater.*, Vol. 104, 2017, pp. 121–138. https://doi.org/10.1016/j.mechmat.2016.10.008.

[19] Liu, Z., Bessa, M., and Liu, W. K., "Self-Consistent Clustering Analysis: An Efficient Multi-Scale Scheme for Inelastic Heterogeneous Materials," *Comput. Methods Appl. Mech. Eng.*, Vol. 306, 2016, pp. 319–341. https://doi.org/10.1016/j.cma.2016.04.004.

[20] He, C., Ge, J., Lian, Y., Geng, L., Chen, Y., and Fang, D., "A concurrent three-scale scheme FE-SCA2 for the nonlinear mechanical behavior of braided composites," *Comput. Methods Appl. Mech. Eng.*, Vol. 393, 2022, p. 114827. https://doi.org/10.1016/j.cma.2022.114827.

[21] Yvonnet, J., and He, Q.-C., "The reduced model multiscale method (R3M) for the non-linear homogenization of hyperelastic media at finite strains," *J. Comput. Phys.*, Vol. 223, No. 1, 2007, pp. 341–368. https://doi.org/10.1016/j.jcp.2006.09.019.

[22] Hernández, J. A., Oliver, J., Huespe, A. E., Caicedo, M. A., and Cante, J. C., "High-performance model reduction techniques in computational multiscale homogenization," *Comput. Methods Appl. Mech. Eng.*, Vol. 276, 2014, pp. 149–189. https://doi.org/10.1016/j.cma.2014.03.011.

[23] van Tuijl, R. A., Harnish, C., Matouš, K., Remmers, J. J. C., and Geers, M. G. D., "Wavelet based reduced order models for microstructural analyses," *Comput. Mech.*, Vol. 63, No. 3, 2019, pp. 535–554. https://doi.org/10.1007/s00466-018-1608-3.

[24] Liu, Z., Wu, C. T., and Koishi, M., "A deep material network for multiscale topology learning and accelerated nonlinear modeling of heterogeneous materials," *Comput. Methods Appl. Mech. Eng.*, Vol. 345, 2019, pp. 1138–1168. https://doi.org/10.1016/j.cma.2018.09.020.

[25] Huang, T., Liu, Z., Wu, C. T., and Chen, W., "Microstructure-guided deep material network for rapid nonlinear material modeling and uncertainty quantification," *Comput. Methods Appl. Mech. Eng.*, Vol. 398, 2022, p. 115197. https://doi.org/10.1016/j.cma.2022.115197.

[26] Dvorak, G. J., "Transformation Field Analysis of Inelastic Composite Materials," *Proc. R. Soc. Lond. A*, Vol. 437, 1992, pp. 311–327.

[27] Oskay, C., and Fish, J., "Eigendeformation-Based Reduced Order Homogenization for Failure Analysis of Heterogeneous Materials," *Comput. Methods Appl. Mech. Eng.*, Vol. 196, No. 7, 2007, pp. 1216–1243. https://doi.org/10.1016/j.cma.2006.08.015.

[28] Zhang, X., and Oskay, C., "Eigenstrain Based Reduced Order Homogenization for Polycrystalline Materials," *Comput. Methods Appl. Mech. Eng.*, Vol. 297, 2015, pp. 408–436. https://doi.org/10.1016/j.cma.2015.09.006.

[29] Zhang, X., and Oskay, C., "Sparse and Scalable Eigenstrain-Based Reduced Order Homogenization Models for Polycrystal Plasticity," *Comput. Methods Appl. Mech. Eng.*, Vol. 326, 2017, pp. 241–269. https://doi.org/10.1016/j.cma.2017.07.027.

[30] Liu, Y., Zhang, X., Zhu, Y., Hu, P., and Oskay, C., "Dislocation density informed eigenstrain based reduced order homogenization modeling: verification and application on a titanium alloy structure subjected to cyclic loading," *Model. Simul. Mater. Sci. Eng.*, Vol. 28, No. 2, 2020, p. 025004. https://doi.org/10.1088/1361-651X/ab602e.

[31] Zhang, X., Liu, Y., and Oskay, C., "Multiscale Reduced-Order Modeling of a Titanium Skin Panel Subjected to Thermomechanical Loading," *AIAA Journal*, Vol. 60, 2021, pp. 302–315. https://doi.org/10.2514/1.J060497.

[32] Xia, D., Zhang, X., and Oskay, C., "Large-deformation reduced order homogenization of polycrystalline materials," *Comput. Methods Appl. Mech. Eng.*, Vol. 387, 2021, p. 114119. https://doi.org/10.1016/j.cma.2021.114119.

[33] Lin, M., Liu, Y., Oskay, C., and Zhang, X., "Microstructure-Informed Reduced-Order Modeling of Fatigue Initiation in a Titanium Skin Panel Subjected to Thermo-Mechanical Loading," *AIAA SCITECH 2022 Forum*, AIAA SCITECH 2022 Forum, 2022. https://doi.org/10.2514/6.2022-0210.

[34] Yuan, Z., and Fish, J., "Are the Cohesive Zone Models Necessary for Delamination Analysis?" *Comput. Methods Appl. Mech. Eng.*, Vol. 310, 2016, pp. 567–604. https://doi.org/10.1016/j.cma.2016.06.023.

[35] Oskay, C., Su, Z., and Kapusuzoglu, B., "Discrete eigenseparation-based reduced order homogenization method for failure modeling of composite materials," *Comput. Methods Appl. Mech. Eng.*, Vol. 359, 2020, p. 112656. https://doi.org/10.1016/j.cma.2019.112656.

[36] Brandyberry, D. R., Zhang, X., and Geubelle, P. H., "A GFEM-based Reduced-Order Homogenization Model for Heterogeneous Materials under Volumetric and Interfacial Damage," *Comput. Methods Appl. Mech. Eng.*, Vol. 377, 2021, p. 113690. https://doi.org/10.1016/j.cma.2021.113690.

[37] Brandyberry, D. R., Zhang, X., and Geubelle, P. H., "Multiscale design of nonlinear materials using reduced-order modeling," *Comput. Methods Appl. Mech. Eng.*, Vol. 399, 2022, p. 115388. https://doi.org/10.1016/j.cma.2022.115388.

[38] Ortiz, M., and Pandolfi, A., "Finite-deformation irreversible cohesive elements for three-dimensional crack-propagation analysis," *Int. J. Numer. Methods Eng.*, Vol. 44, No. 9, 1999, pp. 1267–1282. https://doi.org/10.1002/(SICI)1097-0207(19990330)44:9<1267::AID-NME486>3.0.CO;2-7.

[39] Simo, J. C., and Ju, J. W., "Strain- and stress-based continuum damage models-I. Formulation," *Int. J. Solids Struct.*, Vol. 23, 1987, pp. 821–840. https://doi.org/10.1016/0020-7683(87)90083-7.

[40] Zhang, S., and Oskay, C., "Reduced order variational multiscale enrichment method for elasto-viscoplastic problems," *Comput. Methods Appl. Mech. Eng.*, Vol. 300, 2016, pp. 199–224. https://doi.org/10.1016/j.cma.2015.11.020.

[41] Marfia, S., and Sacco, E., "Computational homogenization of composites experiencing plasticity, cracking and debonding phenomena," *Comput. Methods Appl. Mech. Eng.*, Vol. 304, 2016, pp. 319–341. https://doi.org/10.1016/j.cma.2016.02.007.

[42] Moyeda, A., and Fish, J., "Multiscale analysis of solid, waffle, ribbed and hollowcore reinforced concrete slabs," *Comput. Methods Appl. Mech. Eng.*, Vol. 348, 2019, p. 139–156. https://doi.org/10.1016/j.cma.2019.01.022.

[43] Yu, C., Kafka, O. L., and Liu, W. K., "Self-consistent clustering analysis for multiscale modeling at finite strains," *Comput. Methods Appl. Mech. Eng.*, Vol. 349, 2019, pp. 339–359. https://doi.org/10.1016/j.cma.2019.02.027.

[44] Sparks, P., and Oskay, C., "IDENTIFICATION OF OPTIMAL REDUCED ORDER HOMOGENIZATION MODELS FOR FAILURE OF HETEROGENEOUS MATERIALS," *Int. J. Multiscale Comput. Eng.*, Vol. 11, No. 3, 2013. https://doi.org/10.1615/IntJMultCompEng.2013005373.

[45] Alaimo, G., Auricchio, F., Marfia, S., and Sacco, E., "Optimization clustering technique for PieceWise Uniform Transformation Field Analysis homogenization of viscoplastic composites," *Comput. Mech.*, Vol. 64, No. 6, 2019, pp. 1495–1516. https://doi.org/10.1007/s00466-019-01730-2.

[46] Babuška, I., and Rheinboldt, W. C., "Adaptive Approaches and Reliability Estimations in Finite Element Analysis," *Comput. Methods Appl. Mech. Eng.*, Vol. 17–18, 1979, pp. 519–540. https://doi.org/10.1016/0045-7825(79)90042-2.

[47] Berger, M. J., and Oliger, J., "Adaptive mesh refinement for hyperbolic partial differential equations," *J. Comput. Phys.*, Vol. 53, No. 3, 1984, pp. 484–512. https://doi.org/10.1016/0021-9991(84)90073-1.

[48] Fan, R., Yuan, Z., and Fish, J., "Adaptive Two-Scale Nonlinear Homogenization," *Int. J. Comput. Methods Eng. Sci. Mech.*, Vol. 11, No. 1, 2010, pp. 27–36. https://doi.org/10.1080/15502280903446861.

[49] Ferreira, B. P., Andrade Pires, F., and Bessa, M., "Adaptivity for Clustering-Based Reduced-Order Modeling of Localized History-Dependent Phenomena," *Comput. Methods Appl. Mech. Eng.*, Vol. 393, 2022, p. 114726. https://doi.org/10.1016/j.cma.2022.114726.